JOURNAL OF GUIDANCE, CONTROL, AND DYNAMICS
Vol. 24, No. 3, May–June 2001

Vibration Reduction for Flexible Spacecraft Following Momentum Dumping With/Without Slewing

Arun K. Banerjee* and Nelson Pedreiro†
Lockheed Martin Advanced Technology Center, Palo Alto, California 94304
and
William E. Singhose‡
Georgia Institute of Technology, Atlanta, Georgia 30332

Vibrations following the firing of thrusters to dump wheel momentum degrade pointing performance of a reaction-wheel controlled spacecraft. The use of input shaping is suggested to modulate thruster pulses with a set of properly timed impulses to suppress vibrations after dumping momentum. An exact solution is obtained for thruster switching times in the idealized case of no constraints. With realistic constraints on the thruster, permissible attitude error, and elastic deflection, an optimization problem is solved. The solution is a modification of a concatenated set of pulses for the idealized case, each set designed to dump a fraction of the total momentum with vibration reduction. It is shown that momentum can be dumped during slewing maneuvers along with vibration suppression, resulting in a reduction of slew time with no additional fuel consumption. In this case input shaping is applied to both reaction wheel and thruster commands to minimize residual vibrations. Results of large angle slewing and momentum dumping with and without reaction wheel saturation are presented for the next generation space telescope.

I. Introduction

FIGURE 1a shows a simple spacecraft with flexible solar panels and a reaction wheel that is used to maintain attitude control of the spacecraft. As a result of opposing disturbance torques, for example, due to solar radiation pressure, the wheel momentum builds up and it is necessary to dump momentum before the wheel reaches its maximum speed. This is commonly done by firing spacecraft on–off thrusters. This action, of course, excites vibration modes of the spacecraft, deteriorating its pointing performance. In this paper, a method is presented to compute thruster switching times to reduce spacecraft vibration after dumping momentum. The method is based on the idea of input shaping,[1] which has been used on many applications such as the shuttle middeck experiment[2] minimum-time slewing[3] and spinup[4] of flexible bodies, end-point tracking of flexible robots,[5] long-reach robotics,[6] and high-technology manufacturing.[7] Input shaping is robust to modeling errors, is simple to apply, and compares favorably against alternative methods based on optimal control,[8] adaptive control,[9] nonlinear inversion,[10] Lyapunov control,[11] and phase plane analysis[12] for vibration suppression of slewing flexible bodies.

The present work uses on–off thrusters with multiple pulses to dump momentum in minimum time while reducing vibrations under constraints on reaction wheel and thruster torques, permissible attitude errors, and elastic deformations. This is effectively a new approach of pulse-width and pulse-frequency modulation, as the examples in the paper will show. The other new problem studied here is that of combining momentum dumping with slewing, with input shaping applied to both reaction wheel and thruster commands to reduce residual vibrations. The motivation for doing the operations simultaneously is twofold: First, there is an obvious saving in time compared to doing them separately and, second, the thrusters can be used not only to dump momentum but also to reduce slew time, as compared to the reaction wheel acting alone, without increase in fuel consumption. The overall increase in spacecraft data-taking time can be significant.

In the sequel, input shaping of momentum dumping is studied first in the idealized case when the reaction wheel control torque can equal or exceed the thruster torque and no spacecraft attitude or appendage deflection constraint is present. This is used as a building block for the case of momentum dumping with realistic constraints of reaction wheel control torque saturating at a lower level than the thruster torque and specified requirements on attitude excursions and elastic deflections. These latter results, together with those for input-shaped slewing, are used for vibration suppression for combined momentum dumping and slewing. Finally, results of large-angle slewing and momentum dumping with and without wheel saturation are given for the proposed next generation space telescope.

II. Momentum Dumping with Vibration Suppression: Idealized Case

Dumping of momentum with on–off thrusters calls for a series of one-sided pulses. It proves insightful to treat a pulse train as a convolution of a step input with a sequence of impulses, in which case the desired pulses can be seen as realizable by an even number n of impulses given in Table 1, where A_i are normalized unity impulses, t_i are the switching times, and the first impulse comes at $t_1 = 0$.

The vibration induced by a pulse train can be determined by the time locations of the leading and trailing edges of the pulses, when the discontinuities in force induce vibration. For the residual vibration following thruster firing to be zero and the result to be robust with respect to errors in the frequency of the vibration to be suppressed, the input-shaping equations of zero residual vibration and zero derivative with respect to frequency must be employed.[1] To suppress vibrations of multiple vehicle modes of frequencies ω_j, one writes for each of $j = 1, \ldots, m$ modes the following equations for the n impulses of unity amplitude A_i at time t_i, as given in Table 1, with the first impulse coming at $t = 0$:

$$\sum_{i=1}^{n} (-1)^{i+1} \sin \omega_j t_i = 0 \tag{1}$$

$$\sum_{i=1}^{n} (-1)^{i+1} \cos \omega_j t_i = 0 \tag{2}$$

Received 26 August 1999; revision received 1 April 2000; accepted for publication 24 July 2000.

*Research Scientist, Consultant. Associate Fellow AIAA.
†Research Scientist, Staff. Senior Member AIAA.
‡Assistant Professor, Mechanical Engineering Department. Member AIAA.

Table 1 Train of impulses used to define thruster pulses by convolution with step input

A_i	t_i
1	t_1
−1	t_2
1	t_3
−1	t_4
⋮	⋮
−1	t_n

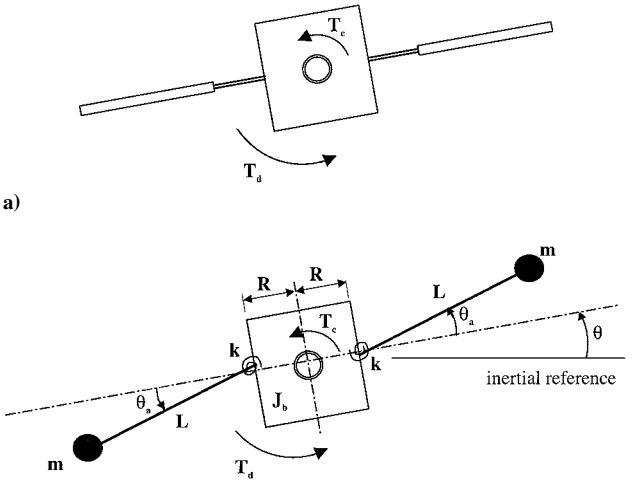

Fig. 1 Simple spacecraft with flexible solar panels and reaction wheel.

Differentiating these equations with respect to frequency provides the robustness condition

$$\sum_{i=1}^{n}(-1)^{i+1}t_i\cos\omega_j t_i = 0 \tag{3}$$

$$\sum_{i=1}^{n}(-1)^{i+1}t_i\sin\omega_j t_i = 0 \tag{4}$$

Let the accumulated momentum of the wheels due to a secular disturbance such as solar radiation pressure be H. The application of input shaping to momentum dumping with thrust of magnitude τ_0 requires the additional constraint

$$\sum_{i=1}^{n}(-1)^{i}t_i - \frac{H}{\tau_0} = 0 \tag{5}$$

Equations (1–5) can be solved exactly for the switching times of the n impulses for the m modes that define the on–off thruster pulse sequence for momentum dumping. The resulting momentum dumping torque is used in the equations of motion of the flexible spacecraft. Figure 1b shows a discrete version of the continuum model of Fig. 1a and is described by the following equations of motion:

$$\left[J_b + 2m(R+L)^2\right]\ddot{\theta} + 2m(R+L)L\ddot{\theta}_a = T_d + T_c \tag{6}$$

$$2m(R+L)L\ddot{\theta} + 2mL^2\ddot{\theta}_a = -2k\theta_a \tag{7}$$

where J_b is the inertia of the spacecraft bus, m is the lumped mass of one appendage, R is the distance from the center of mass of the main body to the attachment point of the massless rods of length L, θ is the spacecraft angle with respect to an inertial frame, θ_a is the appendage angle with respect to the spacecraft, k is a torsional spring constant, T_d is the momentum dumping torque from the thruster, and T_c is reaction wheel control torque. Equations (6) and (7) are of the well-known form of attitude dynamics equations of flexible vehicles with

Table 2 Thruster switching times for momentum dumping with input shaping

A_i	t_i, s
1.0	0
−1.0	0.555
1.0	1.111
−1.0	300.0
1.0	300.555
−1.0	300.111

cantilevered appendages, and the parameters herein can be selected to match the inertia, appendage frequency, and the modal angular momentum coefficient of the continuum spacecraft.[13] Spacecraft disturbances, such as solar torque, which give rise to the buildup of momentum, and reaction wheel disturbances are excluded here so as not to becloud the source of disturbance from the thruster and the environment to the reaction wheel control. It is assumed that the spacecraft attitude errors due to all disturbances can be taken out by a suitably designed reaction wheel control system. In the ideal case, the reaction wheel control torque is permitted to be higher than the thruster torque. Use of a simple proportional integral derivative (PID) control law to describe the torque applied by the wheel on the spacecraft,

$$T_c = -I_w\ddot{\theta}_w = -k_p\theta - k_i\int_0^t \theta\,\mathrm{d}\tau - k_d\dot{\theta} \tag{8}$$

completes the description of the system dynamics, where I_w and θ_w are wheel inertia and angle, respectively. In Eq. (8), the spacecraft angular acceleration has been ignored in comparison with the larger wheel angular acceleration. The following values were selected for the parameters of the simple model shown in Fig. 1b: $J_b = 12{,}800$ kg · m^2, $m = 25$ kg, $R = 2$ m, $L = 10$ m, and $k = 5685$ Nm. These parameters result in a vehicle mode of 0.3 Hz and appendage mode of 0.24 Hz that correspond to the fundamental frequency of an actual spacecraft. Total momentum to be dumped is $H = 81.36$ N · m · s, and the thruster level is 0.2712 N · m. The vibration frequency to be suppressed is taken as 0.3 Hz, and structural damping is taken to be zero. The controller gains for the reaction-wheel-based attitude control are chosen to get a closed-loop bandwidth of 0.03 Hz. Initial wheel speed, representing accumulated angular momentum, is taken to be −6000 rpm. The solution of Eqs. (1–5) for switching times t_i, with A_i given in Table 1, is obtained with a nonlinear equation solver[14] and is given in Table 2.

Note that the thrust pattern consists of two pulses of width 0.555 s before and after a long continuous pulse from 1.111 to 300 s. The two curves in Fig. 2 show the elastic deflection $L\theta_a$ at the tip of the appendage in Fig. 1b for momentum dumping with input shaping and without input shaping, that is, with a step torque for 300 s. Figure 3, which is a plot of Fig. 2 in expanded timescale, shows that the vehicle vibration mode of 0.3 Hz is controlled in a deadbeat manner by input shaping, with the three impulses at the beginning and end of the original 300-s pulse in Table 2. Without input shaping, the vibration is of larger magnitude and persists for longer time because it is only dampened by the PID control. Figure 4a contains the associated wheel speed response, indicating momentum dumping, and is virtually the same for the two cases. The thrust and reaction wheel control torque behaviors with input shaping are given in Fig. 4b for this idealized case, showing that the reaction wheel control torque cancels the thruster torque after an initial transient during which time it exceeds the thrust. Figure 5 uses an expanded timescale to show the details of the thruster and reaction wheel control torque of Fig. 4b near the first and last thruster pulses. These results are based on tuning the shaper to the exact frequency of vibration of the structure, 0.3 Hz. Using the same shaped thruster profile on a structure with a frequency 10% higher than the tuning frequency of the shaper produces the deflection response shown in Fig. 6. The reduction in residual vibration is comparable to that in Fig. 2, and illustrates the robustness of the input-shaping process.

III. Constrained Optimization: Realistic Case

In realistic applications, the reaction wheel control torque has, in general, a saturation level lower than the thruster torque level, and

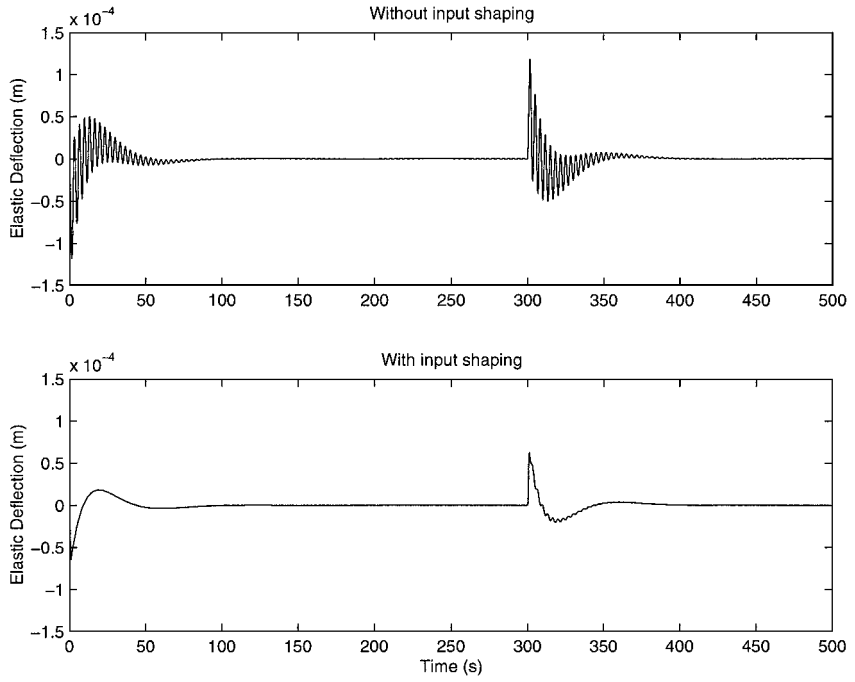

Fig. 2 Appendage deflection for momentum dumping without and with input shaping.

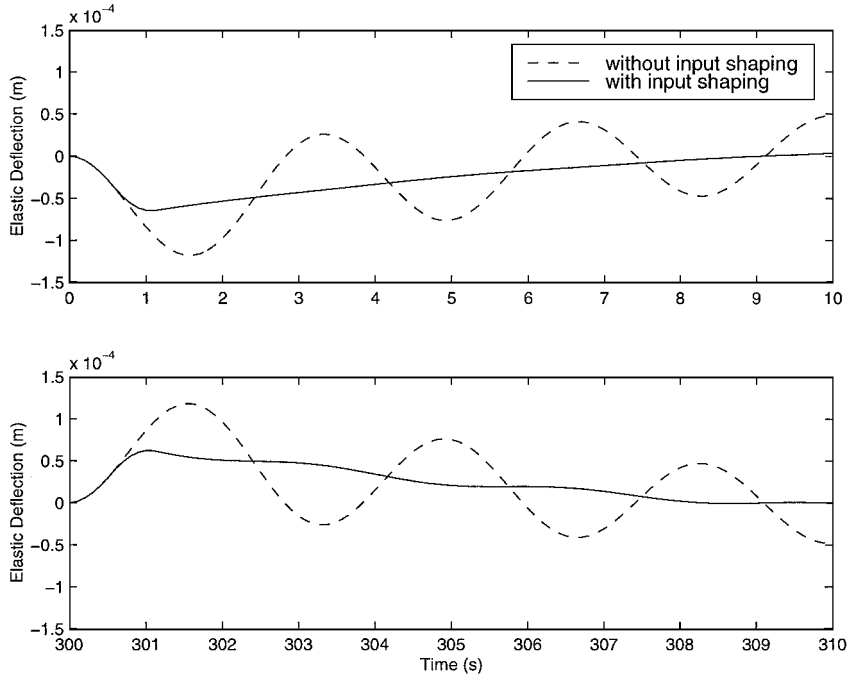

Fig. 3 Details of appendage deflection from Fig. 2.

additional requirements have to be satisfied on the thruster pulse width and frequency, excursions of the spacecraft attitude, and elastic deflections allowed. First, the PID control law of Eq. (8) is replaced with one containing integrator antiwindup[15] to account for control saturation:

$$T_c = -I_w\dot{\theta}_w = -[k_p\theta + k_i\theta_i + k_d\dot{\theta}] \tag{9}$$

$$\dot{\theta}_i = \theta \qquad \text{if} \qquad |T_c| < |T_s|$$

$$\dot{\theta}_i = 0 \qquad \text{if} \qquad |T_c| \geq |T_s| \tag{10}$$

The limited control torque available from the reaction wheels implies that there would be unacceptable attitude errors and elastic deformations at critical points of the structure unless the thruster pulse width is restricted to a maximum value, and an allowable minimum ratio of thruster off and on time is specified. Constraints for a maximum pulse width w are

$$t_1 \leq w, \qquad t_i - t_{i-1} \leq w, \qquad i = 2, \ldots, n \tag{11}$$

Thruster on–off time constraint is stated via a minimum duty cycle ratio R, defined as

$$R \leq (t_2 - t_1)/t_1, \qquad R \leq [(t_i - t_{i-1})/(t_{i-1} - t_{i-2})]$$

$$i = 3, \ldots, n \tag{12}$$

Finally, the constraints of permissible attitude error and elastic deflection are, respectively,

$$\theta_{\max} \leq \theta_0 \tag{13}$$

$$L\theta_{a_{\max}} \leq \delta_0 \tag{14}$$

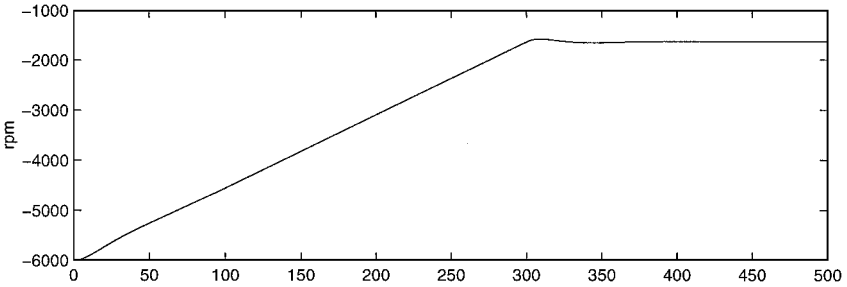

a) Reaction wheel speed

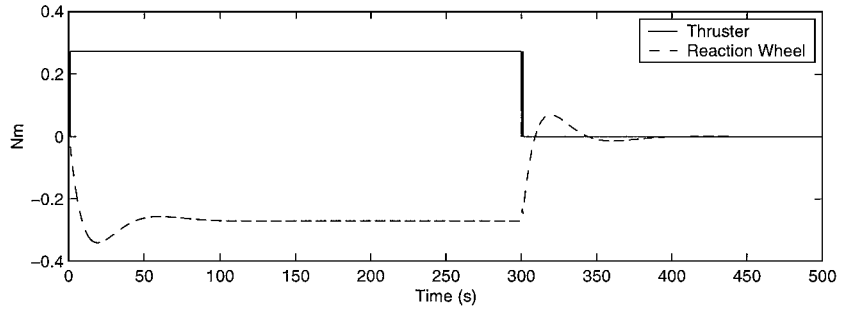

b) Thruster and reaction wheel control torque

Fig. 4 Momentum dumping with input shaping for the idealized case of no constraints on reaction wheel torque.

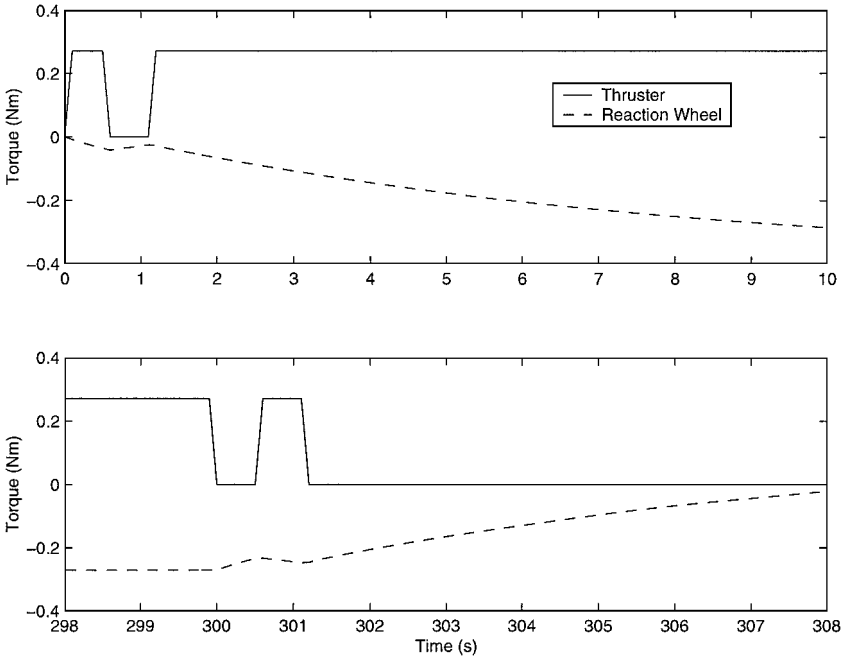

Fig. 5 Details of thruster and reaction wheel control torque from Fig. 4b.

Thruster switching times are now obtained by solving the following constrained optimization problem: Minimize t_n, in the sequence of switching times in Table 1, subject to the vibration suppression equations (1–5), the dynamical equations (6), (7), control equations (8) and (9) and the inequality constraints (10–14). This optimization problem can be solved, for example, using the code ADS.[16] A feasible starting solution is obtained by breaking up the task of total momentum dumping into small fractions, applying the solution for the idealized case to each fractional task, adding a suitable off time for attitude recovery, and then concatenating these solutions.

Thruster on–off times for a momentum dumping torque T_d acting for a duration of t_{on} and an opposing wheel control saturation torque T_c acting for $(t_{on} + t_{off})$ can be calculated so that a rigid body of total inertia J, starting from rest, reaches an attitude excursion of θ_{max} with zero angular velocity:

$$t_{on} = \left(\frac{2\theta_{max}\beta}{\alpha(\alpha + \beta)} \right)^{\frac{1}{2}}, \qquad \alpha \equiv \frac{(T_d - T_c)}{J}, \qquad \beta \equiv \frac{T_c}{J} \tag{15}$$

$$t_{off} = (\alpha/\beta)t_{on} \tag{16}$$

where t_{off} was obtained by setting the net impulse to zero and t_{on} by solving the following equations for maximum attitude angle θ_{max} and zero angular velocity at time t_{max}:

$$\theta_{max} = (\alpha/2)t_{on}^2 + \alpha t_{on}(t_{max} - t_{on}) - (\beta/2)(t_{max} - t_{on})^2 \tag{17}$$

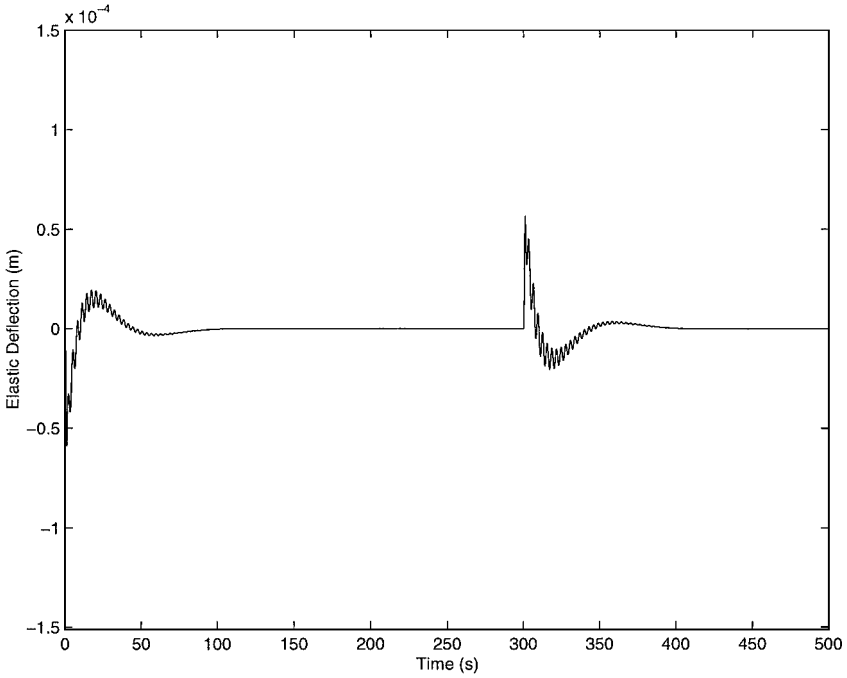

Fig. 6 Appendage elastic deflection with mistuned input shaper, that is, the thrust input profile of Fig. 4b applied to a system with a 10% higher resonant frequency.

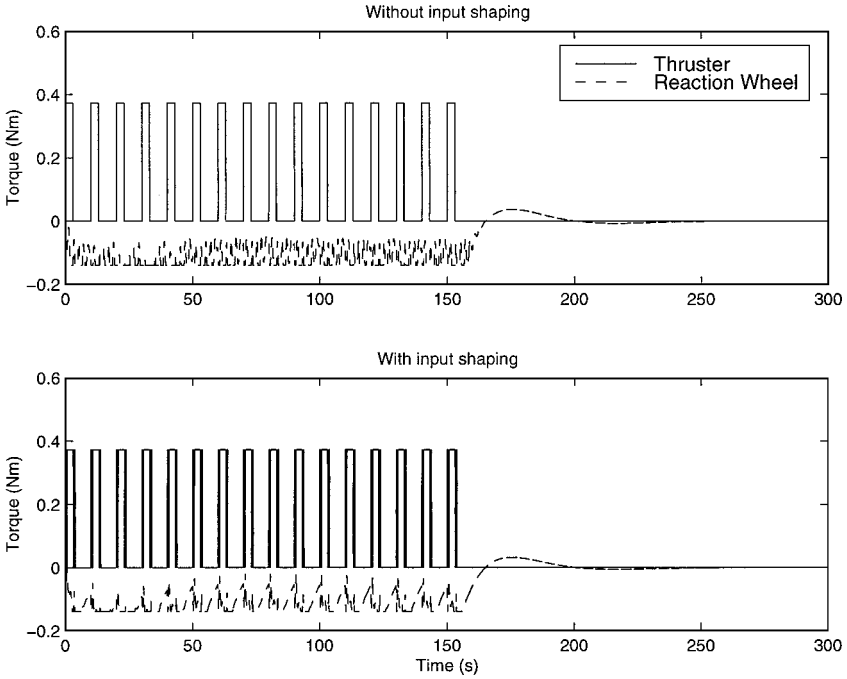

Fig. 7 Thruster and reaction wheel control torque for the realistic case of constraints on available reaction wheel torque and maximum allowable attitude error and elastic deflection, without and with input shaping.

$$0 = \alpha t_{\text{on}} - \beta(t_{\max} - t_{\text{on}}) \tag{18}$$

This basic thrust profile can now be shaped to suppress vibration as in the idealized case and the thruster on–off sequence replicated as needed to achieve the required total momentum to be dumped.

Numerical results are obtained for the simple system shown in Fig. 1b with one elastic mode for the space telescope described later. Spacecraft moment of inertia of 39346 kg · m^2 and vehicle vibration mode with frequency of 0.542 Hz for the simple model are chosen to equal those of a more complex spacecraft described in Sec. V. Thruster torque magnitude is 0.3728 N · m, while the reaction wheel control torque saturation is at 0.14 N · m. Structural damping is taken to be zero. The accumulated momentum can be calculated using well-known relations[17] of the solar radiation force acting at the center of pressure of the solar array. Momentum accumulated over half the satellite orbit period is computed to be 17.89 N · m · s. Attitude error is required to be less than 0.0002 rad and elastic deformation at the appendage node is required to be less than 0.1 mm. Figures 7–12 show the results with and without input shaping. Time histories of thruster pulse firing and wheel torque are shown in Fig. 7, reproduced in greater resolution in Fig. 8 for a time period at the end of the momentum dumping operation. The saturation of the reaction wheel torque can be clearly seen in Fig. 7, and Fig. 8 shows the shaping of the fractional momentum dumping thruster pulses. Figure 9 contains plots of the wheel speed showing momentum dumping. Figure 10 contains the plots of attitude error,

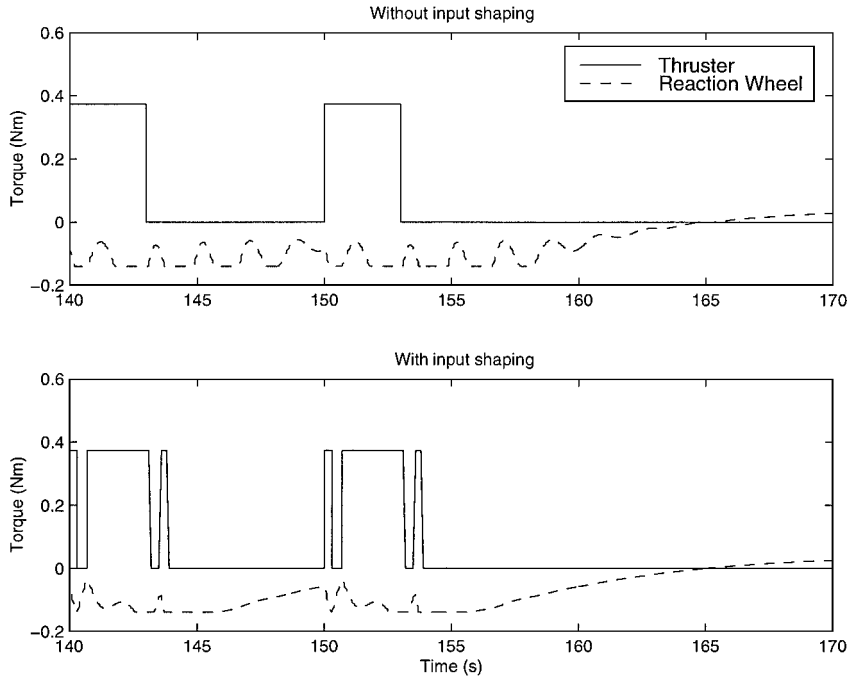

Fig. 8 Details of thruster and reaction wheel control torque from Fig. 7.

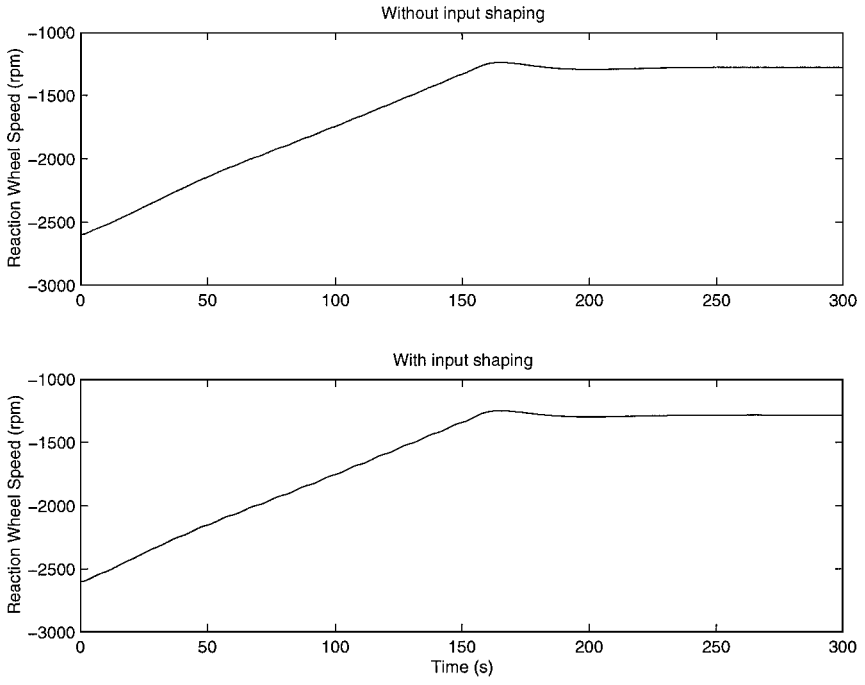

Fig. 9 Momentum dumping without and with input shaping for the case with realistic constraints.

which show a larger violation of the permissible error constraint for the case where input shaping was not used. Figure 11 shows the elastic deformation at a node of interest (mass m in Fig. 1b), the dominant effect of input shaping is clearly seen when the same curves are plotted with expanded timescale in Fig. 12. It is clear that both the vibration and the attitude error are reduced with input shaping.

IV. Vibration Suppression with Combined Momentum Dumping and Slewing

Certain spacecraft, such as space telescopes, require slewing from one orientation to another before any desired data can be collected. Moreover, both slewing and thruster firings excite vibrations that need to damp out before data collection can be resumed. Therefore, the time spent with momentum dumping operations and slewing maneuvers represent interruptions in data-taking time and should be reduced. This can be achieved by combining slewing with momentum dumping, with the stronger disturbance, thruster firing, taking place as early as possible to maximize the time available for attenuation of residual vibrations after slewing. In principle, for a linear system, one can superimpose the actions of thruster firing with input shaping and of slewing with input shaping. It is shown subsequently that one actually gains in overall slewing time by taking advantage of the thrusters in slewing while simultaneously achieving a net momentum dumping at the end of the maneuver. Moreover, no additional fuel consumption is required for the combined momentum dumping and slewing.

When the torque needed for slewing in a desired direction is in the same sense as the desired momentum dumping torque, the thrusters can be used together with the wheel to accelerate the spacecraft, following which the maximum reaction wheel torque is used

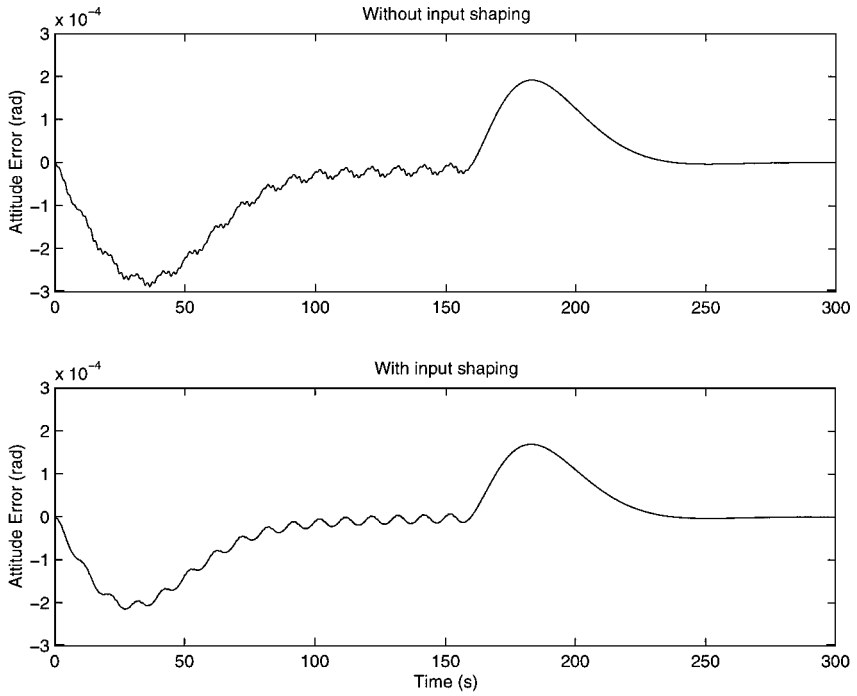

Fig. 10 Attitude error without and with input shaping for the case with realistic constraints.

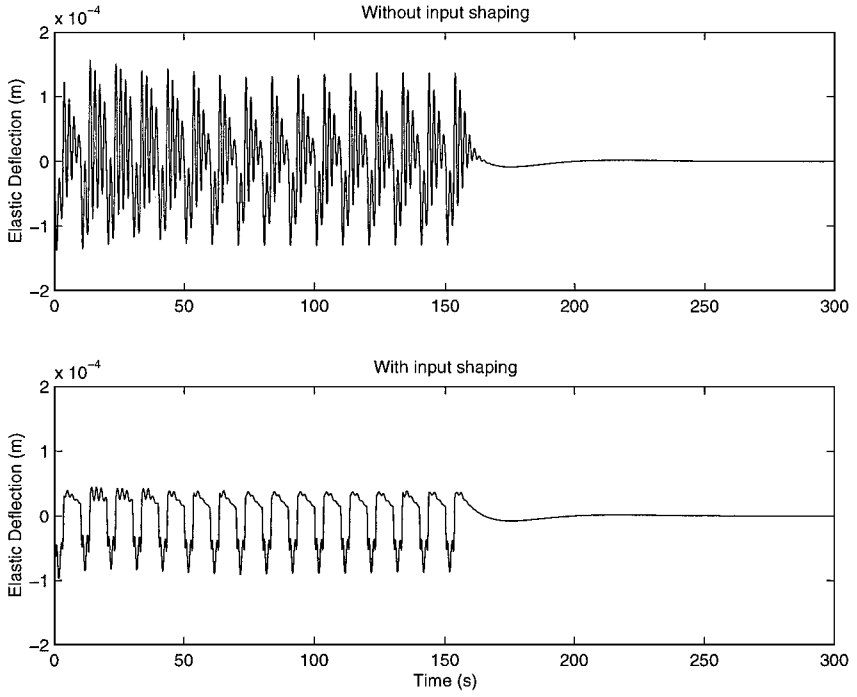

Fig. 11 Appendage deflection showing vibration suppression following momentum dumping due to input shaping for the case with realistic constraints.

to decelerate the spacecraft to rest. During the acceleration phase, wheel torque is applied until the wheel reaches its saturation speed, after which it coasts with zero wheel torque, and finally a reversed wheel torque is applied. If the wheels are saturated at the beginning of the maneuver, then the thrusters alone are used during the acceleration phase. As per this strategy, reaction wheel control switching times are computed as follows. Let

$$\omega_1 = \frac{1}{J}\int_0^{t_1} (T_c + T_d)\,\mathrm{d}\tau \tag{19}$$

$$\theta_1 = \frac{1}{J}\int_0^{t_1}\int_0^{t} (T_c + T_d)\,\mathrm{d}\tau\,\mathrm{d}\tau \tag{20}$$

with T_c the maximum reaction wheel control torque, T_d the momentum dumping (thruster) torque obtained in the preceding section, and t_1 the time at the end of thrusting. Then the switching time t_2, where the reaction wheel torque goes off because of wheel saturation, is calculated from

$$\omega_2 = \omega_1 + \alpha(t_2 - t_1) \tag{21}$$

$$\theta_2 = \theta_1 + \omega_1(t_2 - t_1) + (\alpha/2)(t_2 - t_1)^2 \tag{22}$$

where α is computed from the maximum wheel torque, as in the preceding section. The state at time t_3 denoting end of coasting is calculated from

$$\omega_3 = \omega_2 \tag{23}$$

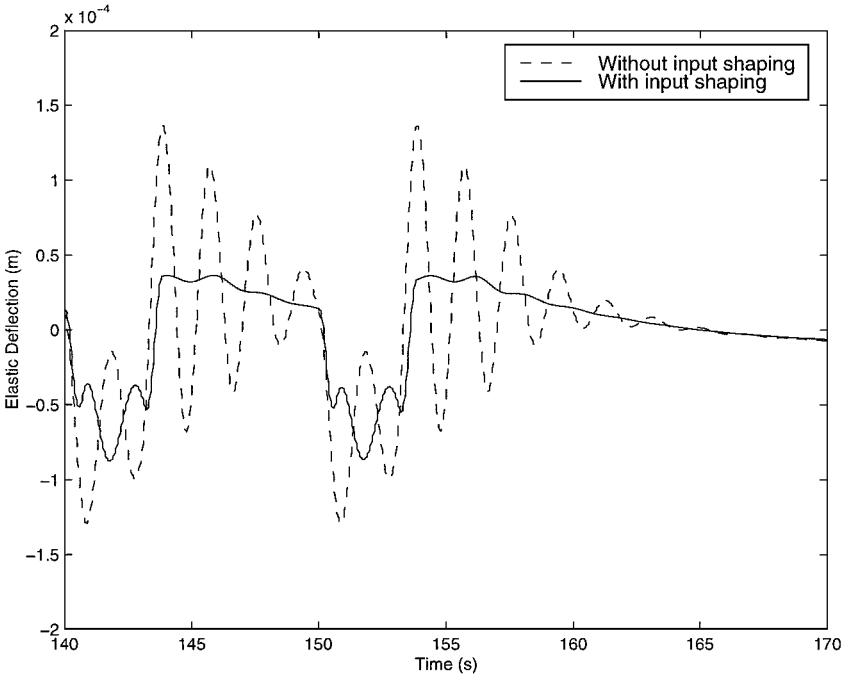

Fig. 12 Details of appendage elastic deflection from Fig. 11.

$$\theta_3 = \theta_2 + \omega_2(t_3 - t_2) \tag{24}$$

Finally, the conditions of slewing to rest at the desired slew angle θ_f require

$$\omega_3 - \alpha(t_4 - t_3) = 0 \tag{25}$$

$$\theta_3 + \omega_3(t_4 - t_3) - (\alpha/2)(t_4 - t_3)^2 = \theta_f \tag{26}$$

In Eqs. (19–26), the only two unknowns, t_3 and t_4, can be solved from Eqs. (25) and (26) because t_1 is known from the net momentum to be dumped and t_2 is known from the difference between the present wheel speed and the saturation speed.

Equations (19–26) correspond to the case where the thruster torque is in the same direction as the slewing acceleration torque. When the thruster torque has to oppose the slewing acceleration torque, the reaction wheel alone provides the acceleration up to time t_1. Then, the thrusters come on together with the reversed wheel torque to provide a rapid deceleration to time $t_1 + \Delta$ when the thrusters go off and the wheel finishes the slewing at time t_2. Knowing Δ, the thruster activity time from Sec. III, one computes times t_1 and t_2 from the following:

$$\omega_1 = \alpha t_1 \tag{27}$$

$$\theta_1 = (\alpha/2)t_1^2 \tag{28}$$

$$\omega_2 = \omega_1 - \int_{t_1}^{t_1+\Delta} \frac{1}{J}(T_c + T_d)\,\mathrm{d}\tau \tag{29}$$

$$\theta_2 = \theta_1 + \omega_1\Delta - \int_{t_1}^{t_1+\Delta}\int_{t_1}^{t} \frac{1}{J}(T_c + T_d)\,\mathrm{d}\tau\,\mathrm{d}\tau \tag{30}$$

$$\omega_2 - \alpha(t_2 - t_1 - \Delta) = 0 \tag{31}$$

$$\theta_2 + \omega_2(t_2 - t_1 - \Delta) - (\alpha/2)(t_2 - t_1 - \Delta)^2 = \theta_f \tag{32}$$

where the integrals in Eqs. (29) and (30) can be evaluated numerically or in the average sense of pulse-width, pulse-frequency modulation, with T_c the maximum control torque and T_d the momentum dumping torque obtained in Sec. III.

Table 3 Three-impulse sequence for input shaping

A_i	t_i
0.25	0
0.5	$T/2$
0.25	T

A PID-type tracking control law with feedforward command is used for slewing. The feedback is turned off for the duration of the thruster firing so that the wheel feedback control does not respond to the oscillations excited by thruster firings:

$$T_c = J\ddot{\theta}_c + k_d(\dot{\theta}_c - \dot{\theta}) + k_p(\theta_c - \theta) + k_i\theta_i \tag{33}$$

$$\dot{\theta}_i = \theta_c - \theta \quad \text{if} \quad |T_c| < |T_s|$$

$$\dot{\theta}_i = 0 \quad \text{if} \quad |T_c| \geq |T_s| \tag{34}$$

where $\ddot{\theta}_c$, $\dot{\theta}_c$, and θ_c are the commanded angular acceleration, velocity, and position, respectively, computed using Eqs. (19–26) or (27–32). In Eq. (33), $J\ddot{\theta}_c$ represents the feedforward torque command, which being discontinuous would induce vibrations. To suppress these vibrations in a robust manner, it is necessary to preshape the command input by a convolution of the slewing acceleration profile with the well-known three impulse sequence,[1] shown in Table 3 for a vibration mode of period T.

The results of convolution of the three-impulse sequence with the required reaction wheel acceleration command given in Eqs. (27–32) are

$$\ddot{\theta}_c = 0.25\alpha_{\max}, \qquad 0 \leq t \leq T/2 \tag{35a}$$

$$\ddot{\theta}_c = 0.75\alpha_{\max}, \qquad T/2 \leq t \leq T \tag{35b}$$

$$\ddot{\theta}_c = \alpha_{\max}, \qquad T \leq t \leq t_1 \tag{35c}$$

$$\ddot{\theta}_c = 0.5\alpha_{\max}, \qquad t_1 \leq t \leq t_1 + T/2 \tag{35d}$$

$$\ddot{\theta}_c = -0.5\alpha_{\max}, \qquad t_1 + T/2 \leq t \leq t_1 + T \tag{35e}$$

$$\ddot{\theta}_c = -\alpha_{\max}, \qquad t_1 + T \leq t \leq t_3 \tag{35f}$$

$$\ddot{\theta}_c = -0.75\alpha_{\max}, \qquad t_3 \leq t \leq t_3 + T/2 \tag{35g}$$

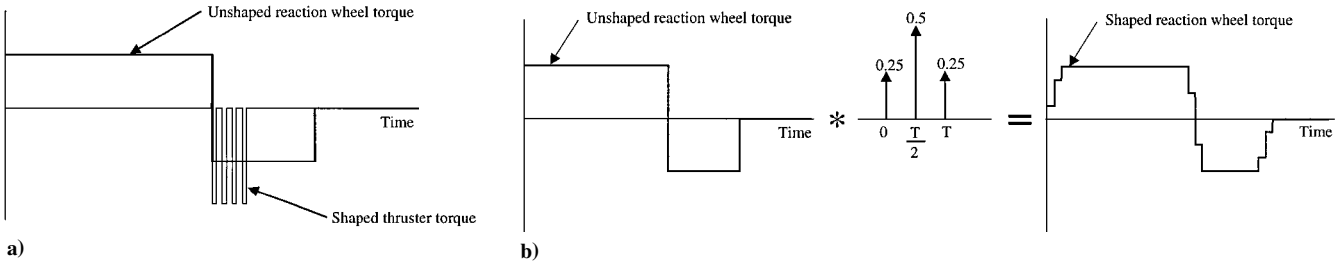

Fig. 13 Process of combined momentum dumping and slewing with vibration suppression.

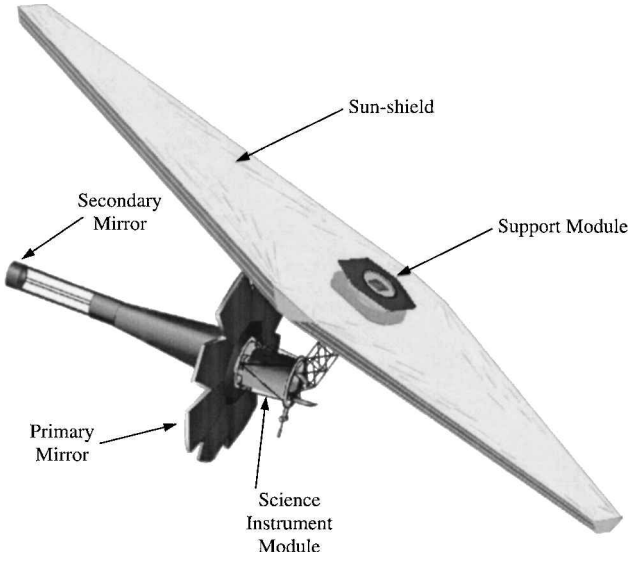

Fig. 14 NASA concept for NGST.[18]

$$\ddot{\theta}_c = -0.25\alpha_{\max}, \qquad t_3 + T/2 \le t \le t_3 + T \tag{35h}$$

$$\ddot{\theta}_c = 0, \qquad t_3 + T \le t \tag{35i}$$

The concept of combined momentum dumping and slewing with vibration suppression is shown in Fig. 13. Figure 13a shows the influence of shaped momentum dumping on generating the unshaped reaction wheel torque, given by Eqs. (27–32); Fig. 13b shows the convolution operation of Eqs. (35) used to shape the reaction wheel torque to suppress residual vibrations.

V. Application to a Complex Spacecraft

An illustration of the NASA concept for the next generation space telescope[18] (NGST) is shown in Fig. 14. The concept calls for a lightweight space observatory with an 8-m segmented primary mirror. Shown in Fig. 14 are the primary and secondary mirrors, the science instrument module, the support module (containing solar panels, reaction wheels, thrusters, and other mission support equipment) and the sunshield. Overall, the proposed NGST observatory is a large lightweight structure with significant portions of the structure operating at cryogenic temperatures. As a consequence, vibrations that are excited by thruster firings and slewing maneuvers can take a long time to damp out, significantly impacting the time available for conducting astronomical observations. In this case, the proposed combination of momentum dumping with slewing maneuvers can provide significant increase in observation time, due not only to the evident time savings achieved by combining the two operations but also to the ability of performing faster slews with no additional fuel consumption.

Figure 15 shows a top-level block-diagram of the attitude control and image stabilization proposed for NGST. The command generator receives inputs from mission control for observatory retargeting and momentum dumping and generates trajectory commands to the

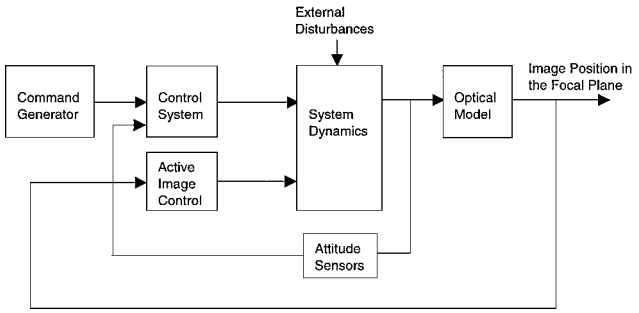

Fig. 15 Top-level block diagram for NGST attitude control and image stabilization.

attitude control loop as well as thruster commands. The architecture used for the fine pointing control system is similar to the one proposed by Mosier et al.[19] The attitude control loop consists of feedforward and feedback control logic similar to the one described in the preceding section; gyros and star trackers are used for inertial attitude sensing and a reaction wheel assembly (RWA) is used to apply control torque to the spacecraft. The outputs of the control system are torque commands to the RWA and thruster commands. Included in the model of the system are spacecraft rigid- and flexible-body dynamics, dynamics of the RWA, and the dynamics of a two-axis steering mirror used for active image control. The optical model used in the simulations is an optical sensitivity matrix relating displacements of optical elements to image motion in the focal plane, which represents the performance metric used in the analysis. For NGST, the main external disturbance is the solar torque, which will cause momentum buildup on the RWA. Modal cost analysis[20] was used to rank the modes, with the top five modes selected to represent the flexible-body dynamics. Only the most disturbable vehicle mode, of 0.542 Hz, was used in the equivalent simple model of Fig. 1b, with zero damping, to generate the shaped thruster switching times computed earlier. These same switching times are retained for the complex model with many modes. To isolate the effects of slew and thruster induced vibrations, the disturbances caused by static and dynamic imbalance of the reaction wheels and the active image motion compensation were not included in the simulations.

The results of vibration reduction with simultaneous momentum dumping and slewing for the NGST spacecraft are given in Figs. 16 and 17. Figure 16 is for slewing in the same direction that the momentum dumping thruster would cause the spacecraft to rotate. It shows the thruster and reaction wheel torque in Fig. 16a, and the wheel angular momentum in Fig. 16c, showing the period of coasting with no wheel torque as the wheel speed reaches its saturation level. The resulting −60-deg slewing profile is given in Fig. 16b. Results for slewing in the opposite direction to the rotation caused by the momentum dumping torque are given in Fig. 17. Figure 17a shows the thruster and reaction wheel torques, Fig. 17b shows the 60-deg slewing response, and Fig. 17c shows the wheel momentum. Figure 18 shows evolution with time of the focal plane X and Y components of image motion and also snapshots of the projection of this motion in the focal plane. The results refer to the simultaneous slew and momentum dumping shown in Fig. 17. Because the

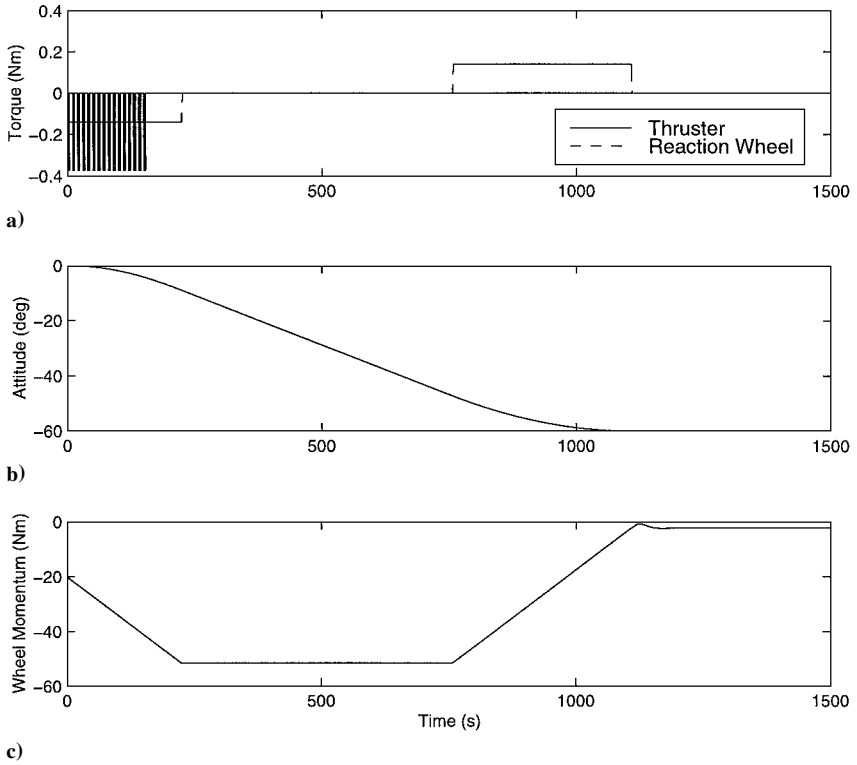

Fig. 16 Combined slewing and momentum dumping for NGST with reaction wheel saturation.

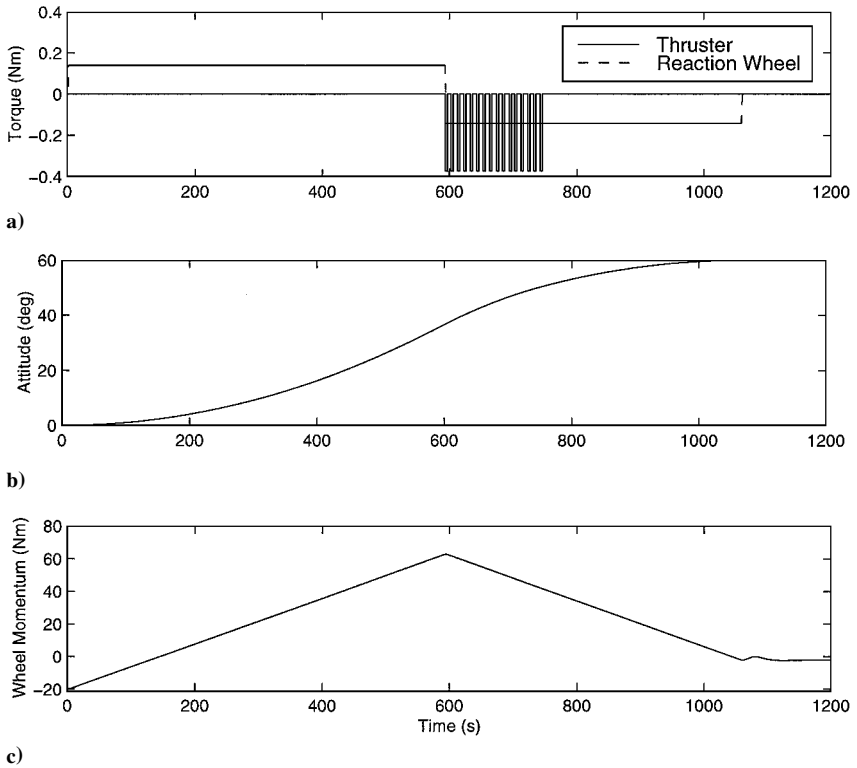

Fig. 17 Combined slewing and momentum dumping for NGST without reaction wheel saturation.

image motion in the focal plane is affected by the deflections and rotations of all nodes representing the optical elements of the system, Fig. 18 gives a measure of the vibration attenuation of the overall structure. For the parameters of the system under consideration, the total slewing time, with momentum dumping started in the latter half of slewing, is 1017 s. In comparison, the minimum time for shaped bang–bang slewing with reaction wheel alone is 1097 s. It is seen that using the thrusters together with the wheels has reduced the slewing time, and the fuel consumption is the same as if momentum dumping had been carried out without slewing. The reduction of approximately 7% in slew time is limited by the thruster torque capability, that is, if larger torque is available from the thrusters the slew time decreases further. For the proposed NGST spacecraft, simultaneous rather than separate momentum dumping and slewing translates directly into more time available for astronomical observations.

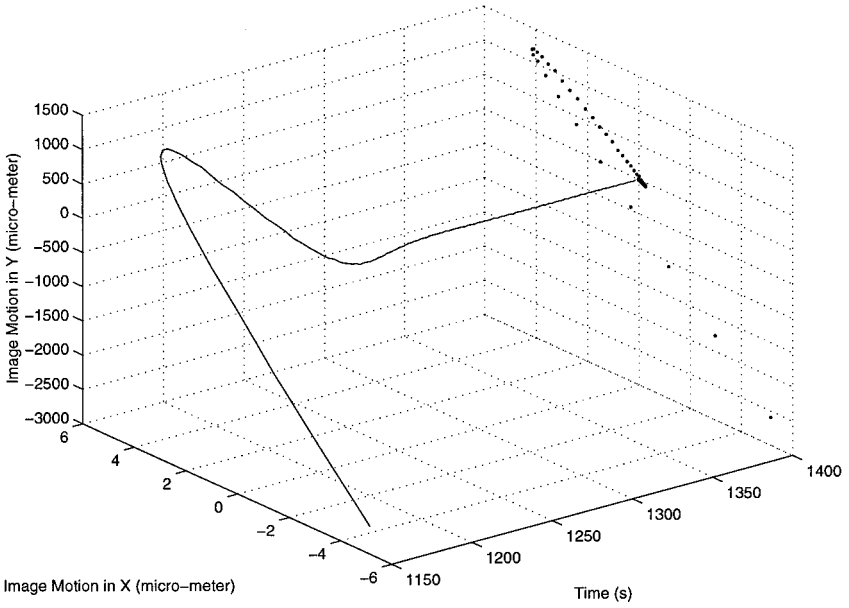

Fig. 18 Image motion evolution and projection on focal plane for combined slewing and momentum dumping.

VI. Conclusions

Vibration reduction following momentum dumping by on–off thrusters on a flexible spacecraft has been demonstrated. The method consists of solving an optimization problem for the thruster switching times. The optimizer minimizes the final switching time subject to the constraints of vibration suppression, momentum to be dumped, thruster pulse width and off time, permissible attitude error due to thruster firing, and allowable elastic deformation of an appendage. The solution is a modification of a concatenated set of solutions of fractional momentum dumping with vibration suppression for the case of no constraints. Robustness of the procedure rests on the well-known derivative constraints of input shaping. Strategies for simultaneous momentum dumping and slewing are given, where advantage is taken of the thrusters to reduce the slewing time below the minimum time for reaction wheel control acting by itself without additional fuel consumption. Two cases of large-angle slewing are demonstrated, one accommodating reaction wheel saturation, for momentum dumping torque helping and opposing slewing in the required direction. Numerical simulations show the feasibility of the approach for vibration attenuation following momentum dumping with or without slewing for precision flexible spacecraft such as the proposed NGST.

Acknowledgments

We thank the reviewers, and particularly the Associate Editor, Hari Hablani, whose insightful comments led to a substantial improvement in the exposition of the paper.

References

[1]Singer, N. C., and Seering, W. P., "Preshaping Command Inputs to Reduce System Vibration," *Journal of Dynamic Systems, Measurement, and Control*, Vol. 112, No. 3, 1990, pp. 76–82.

[2]Tuttle, T., and Seering, W., "Creating Time Optimal Commands with Practical Constraints," *Journal of Guidance, Control, and Dynamics*, Vol. 22, No. 2, 1999, pp. 241–250.

[3]Singhose, W., Banerjee, A., and Seering, W., "Slewing Flexible Spacecraft with Deflection-Limiting Input Shaping," *Journal of Guidance, Control, and Dynamics*, Vol. 20, No. 2, 1997, pp. 291–298.

[4]Banerjee, A. K., "Dynamics and Control of the WISP Shuttle-Antennae System," *Journal of Astronautical Sciences*, Vol. 41, No. 1, 1993, pp. 73–90.

[5]Banerjee, A. K., and Singhose, W. E., "Command Shaping in Tracking Control of a Two-Link Flexible Robot," *Journal of Guidance, Control, and Dynamics*, Vol. 21, No. 6, 1998, pp. 1012–1015.

[6]Magee, D. P., and Book, W. J., "Filtering Micro-Manipulator Wrist Commands to Prevent Flexible Base Motion," American Control Conference, American Automatic Control Council, Green Valley, AZ, 1995, pp. 924–928.

[7]Jones, S., and Ulsoy, A. G., "An Approach to Control Input Shaping with Application to Coordinate Measuring Machines," *Journal of Dynamic Systems, Measurement and Control*, Vol. 121, No. 6, 1999, pp. 242–247.

[8]Liu, Q., and Wie, B., "Robust Time Optimal Control of Uncertain Flexible Spacecraft," *Journal of Guidance, Control, and Dynamics*, Vol. 15, No. 3, 1992, pp. 597–604.

[9]Sasiadek, J. Z., and Srinivasan, R., "Dynamic Modeling and Adaptive Control of a Single-Link Flexible Manipulator," *Journal of Guidance, Control, and Dynamics*, Vol. 12, No. 6, 1989, pp. 838–844.

[10]De Luca, A., and Siciliano, B., "Trajectory Control of a Nonlinear One-Link Flexible Arm," *International Journal of Control*, Vol. 50, No. 5, 1989, pp. 1699–1715.

[11]Junkins, J. L., Rahman, Z. H., and Bang, H., "Near-Minimum Time Control of Distributed Parameter Systems: Analytical and Experimental Results," *Journal of Guidance, Control, and Dynamics*, Vol. 14, No. 2, 1991, pp. 406–415.

[12]Hablani, H. B., "Zero-Residual-Energy, Single-Axis Slew of Flexible Spacecraft Using Thrusters: Dynamics Approach," *Journal of Guidance, Control, and Dynamics*, Vol. 15, No. 1, 1992, pp. 104–113.

[13]Hughes, P. C., "Modal Identities for Elastic Bodies, with Application to Vehicle Dynamics and Control," *Journal of Applied Mechanics*, Vol. 47, March 1980, pp. 177–184.

[14]Kane, T. R., and Levinson, D. A., *AUTOLEV User's Manual*, Online Dynamics, Sunnyvale, CA, July 1999.

[15]Franklin, G. F., Powell, J. D., and Emami-Naeini, A., *Feedback Control of Dynamic Systems*, Addison Wesley Longman, Reading, MA, 1986, pp. 100–103.

[16]Vanderplaats, G. N., "ADS—A Fortran Program for Automated Design Synthesis, Ver. 2.01," User's Manual, Engineering Design Optimization, Santa Barbara, CA, 1987.

[17]Agrawal, B. N., *Design of Geosynchronous Spacecraft*, Prentice–Hall, Upper Saddle River, NJ, 1986, pp. 133–135.

[18]Bely, P.-Y., "NGST Yardstick Mission," *Proceedings of the 1998 34th Liege International Astrophysics Colloquium*, SP-429 ESA, Noordwijk, The Netherlands, 1998, pp. 159–166.

[19]Mosier, G., Femiano, M., Ha, K., Bely, P., Burg, R., Redding, D., Kissil, A., Rakoczy, J., and Craig, L., "Fine Pointing Control for a Next Generation Space Telescope," *Space Telescopes and Instruments V*, Vol. 3356, International Society for Optical Engineering, Kona, Hawaii, March 1998, pp. 1070–1077.

[20]Skelton, R. E., Hughes, P. C., and Hablani, H. B., "Order Reduction for Models of Space Structures Using Modal Cost Analysis," *Journal of Guidance and Control*, Vol. 5, No. 4, 1982, pp. 351–357.